Regular article

Flow-injection responses of diffusion processes and chemical reactions

Jens E.T. Andersen

Department of Chemistry, Technical University of Denmark, Building 207, DK-2800 Lyngby, Denmark

Abstract. The technique of flow-injection analysis (FIA), now 25 years old, offers unique analytical methods that are fast, reliable and consume an absolute minimum of chemicals. These advantages together with its inherent feasibility for automation warrant the future application of FIA as an attractive tool of automated analytical chemistry. The need for an even lower consumption of chemicals and for computer analysis has motivated a study of the FIA peak itself, i.e., a theoretical model that provides detailed knowledge of the FIA profile was developed. It was shown that the flow in a FIA manifold may be characterised by a diffusion coefficient that depends on the flow rate, denoted as the kinematic diffusion coefficient. The description was applied to systems involving species of chromium, both in the case of simple diffusion and in the case of chemical reaction. It is suggested that the description may be used in the resolution of FIA profiles to obtain information about the content of interferences, in the study of chemical reaction kinetics and to measure absolute concentrations within the FIA-detector cell.

Key words: Flow-injection analysis – Diffusion – Kinetics – Analytical chemistry – Theory

1 Introduction

Originally, the flow-injection analysis (FIA) technique was developed to fulfil a demand for automated, fast and reliable chemical analysis [1, 2]. Less emphasis was put on the low consumption of chemicals but this, of course, is closely linked to the ability of FIA to maintain a high frequency of analysis; several hundred samples may be analysed per hour with small statistical errors. Recent developments of FIA show that even smaller amounts of chemicals were consumed by exploiting the facilities of computers and interfaces. By sequential-injection analysis [3] the sample injection was performed by a computer-controlled valve which, in addition, eliminates the errors of manual injection. Micro-FIA systems have been made with dimensions in the micron range, i.e., the diameter of the tubing is a few micron using nanolitre analytical volumes [4, 5]. Such advances are important not only to maintain a low consumption of chemicals but are also important for sample analysis of very rare or expensive analytes.

Many descriptions of the physics of FIA are available and they all convey some profoundly different views on the flow process itself [6]. The aim of modelling FIA is to predict favourable dimensions and conditions of the system, to optimise the system without performing an extensive number of experiments. In addition, if the dominating physical mechanisms were uncovered, it would facilitate comparison of diffusion constants and, eventually, lead to better understanding of the chemical reaction kinetics in a system subjected to flow conditions.

In a pioneering work, Nagy et al. [7] showed that for a signal of an electrochemical response, the FIA peak area was proportional to the inverse flow rate. Korenaga et al. [8] proposed a model of pure Poiseuille flow with and without molecular diffusion and they predicted that the tail of the FIA signal decreases as the reciprocal of the time. Narusawa [9] extended the FIA model of Poiseuille flow by including axial dispersion and axial diffusion as well as radial dispersion and radial diffusion. A model proposed by Vanderslice et al. [10] included detailed studies of the diffusion process which is founded on the convective-diffusion equation and, in this treatment, the time of arrival of the peak leading edge as well as the residence time become proportional to the square of the channel (tube) radius. In a study by Hulsman et al. [11] solid particles of micron dimensions are injected in a FIA manifold as a "solute" in a buffer carrier. Greater retention times were found for the large-sized particles compared with those of dye solutions, and it was found that the retention time depend on the particle density [11]. In the present work a new method of treating the FIA experiment is introduced. The aim of the theory developed in the present work is to determine the precise concentration profile, at all times, within the segment confined by the volume of solute molecules. By assuming simple first-order diffusion, the FIA response

may be described by mathematical convolution of diffusing molecules within a segment. A new diffusion coefficient that depends on the flow rate emerges from fitting the theory to experimental studies of chromium species.

2 Experimental

2.1 Chemicals

The solutions of pure chromium species, used for the study of diffusion without chemical reactions, were prepared from analytical grade $Cr(No_3)_3 \cdot 9H_2O$ (Merck) and K_2CrO_4 (Merck) in distilled water. The concentrations were 0.02 M and 0.001 M for Cr^{3+} and chromate, respectively. These concentrations were chosen in order to obtain reasonably sized FIA peak heights in a wide range of flow rates and coil lengths.

In order to exemplify modelling of a chemical reaction by theory, the reaction between chromate and diphenylcarbazide (DPC) [12, 13] was studied. These experiments included only chromate species. A chromate solution with a concentration of 2 mg/l was injected into a carrier of distilled water and reagent. The reagent was prepared by dissolving 0.75 g DPC in 0.4 l ethanol followed by dilution to a total volume of 1 l with 0.6 M sulphuric acid.

2.2 FIA system

The FIA manifold consisted of an injection valve, a straight tube and a 1-mm detector. In order to exclude turbulence and to ensure that laminar flow prevailed 1-mm straight tubes were used throughout (also within the valve). The experiments were performed with a UV/vis spectrophotometric detector (Hewlett-Packard, HP8452) using a FIA manifold with peristaltic pumps (Ismatec). The injected samples were analysed by photometric detection at 400 nm both for the Cr^{3+} species and for the chromate species. This slightly "off-peak" wavelength (400 nm) was chosen because both species absorb very well and because any dependence on wavelength was excluded from the study of pure diffusion. The peak absorbance at 548 nm was chosen for the chromium – DPC product.

For the samples of Cr^{3+} ions, a 45-μl injection volume was used while the injection volume of chromate was 132 μl. Tube diameters of 0.5 mm and injection volumes of 30 μl were used in the experiments with chromium – DPC. Distilled water was used as a carrier. The detection of the species was performed in a flow cell with a volume of 8 μl and a length of 1 cm.

3 Results and discussion

3.1 Segment flow with molecular diffusion in tubes

In the following derivation a number of assumptions are introduced with the purpose of simplifying the description.

1. It is assumed that the detector response is rapid and that it registers any change in absorbance. The response must be much faster than the characteristic time of diffusion. Termed differently, the change in concentration in the detector cell must be slow compared to the time the detector needs to register a change in absorbance.

2. The flow is laminar at low Reynolds numbers and ions or molecules of the solute follow the streamlines of the solvent. The type of laminar flow includes the possibility of "pluglike" flow with a single flow rate assigned to all streamlines. Phenomena such as microturbulence,

boundary layers and radial diffusion are omitted, to a first approximation.

3. The diffusion of ions and molecules follows Fick's first law. The time-dependent concentration, $c(t)$, may then be described by $c(t) = c_0 \exp(Bt)$, where c_0 is the concentration of the injection volume and B is the diffusion parameter (with units of s^{-1} and $B < 0$).

4. The midsection of the solute segment travels at the speed of the linear flow rate,

$$v_x = \frac{\partial x}{\partial t} = \frac{\partial V}{\partial t} (\pi r_0^2)^{-1} \; ,$$

where $\partial V/\partial t$ is the measured volumetric flow rate and r_0 is the radius of the tubes.

5. The solvent is incompressible.

These assumptions strictly define the type of flow and it is possible to characterise in detail the response observed by the detector. First, we consider the segment before injection: in this state, the segment has the length L_0 and contains a solute with concentration c_0. Thus, the concentration may also be expressed as

$$c_0 = \frac{N_0}{\pi r_0^2 L_0} \; ,$$

where N_0 denotes the number of ions or molecules in the volume. After injection the concentration is given by

$$c(t) = \frac{N_0}{\pi r_0^2 L_0} \exp(Bt) \; .$$

Thus, the Beer–Lambert equation takes the form

$$A(t) = \varepsilon l c(t) = \varepsilon l c_0 \exp[Bt] = A_0 \exp[Bt] \; , \tag{1}$$

where ε is the absorptivity and l is the length of the cell. Because the number of molecules within the segment during the flow is constant, the segment expands in length as a function of time according to

$$L(t) = L_0 \exp(-Bt) \; , \tag{2}$$

which shows that the extension of the segment increases exponentially with time. The shape of the segment during flow is shown schematically in Fig. 1. If the length of the segment increases exponentially, the mixing of solute with solvent may be uniform (Fig. 1), and produces no concentration gradients within the volume
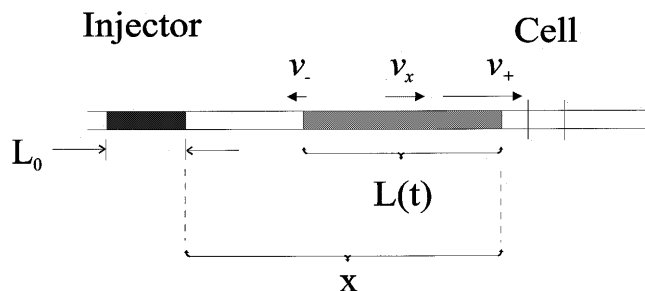
Fig. 1. Schematic illustration of the flow-injection analysis (FIA) experiment. The segment, of initial length L_0, is injected into the carrier stream and evolves in length $L(t)$, as a function of time according to exponential diffusion (Eq. 1). The velocities associated with the front and tail are indicated by v_+ and v_-, respectively. The midsection of the segment travels as the linear flow rate (v_x)

of the segment. Alternatively, if the mixing of solute and solvent proceeded by solvent molecules entering the volume confined by the solute molecules, a nonuniform distribution of solute molecules would result.

3.2 Determination of the maximum sampling frequency

Since the midsection of the segment travels with the speed of the linear flow rate, the front of the segment travels at a higher speed given approximately by the sum of the translatory velocity, v_x, and the diffusive velocity, v_d, i.e., $v_+ = v_x + v_d$.

$$v_+ = v_+ + v_d = v_x + \frac{1}{2}\frac{\partial L(t)}{\partial t} = v_x - \frac{L_0}{2}B\exp[-Bt] \ . \quad (4)$$

The total distance, $x_+(t)$, covered by the front of the segment as a function of time is found by integration of Eq. (4).

$$x_+(t) = \tfrac{1}{2}L_0[\exp(-Bt) - 1] + v_x t \ . \quad (5)$$

When the distance where the front of the segment reaches the detector is x_0, the time of onset may be determined by setting $x_+(t) = x_0$ in the transcendent equation of Eq. (5). By expanding Eq. (5) to first order, the approximate time of arrival of the leading edge becomes

$$t_0 \cong \frac{2x_0}{2v_x - BL_0}, \quad 0 < -Bt_0 < 1 \ . \quad (6)$$

The time values of Eqs. (4)–(6) contain information vital for the understanding of the flow process and they may be applied to a comparison with prediction of, for example, the Poiseuille model. The time of onset, as predicted by Korenaga et al. [8] using the Poiseuille model, is given by half the value of the time calculated by the measured discharge, i.e., $t_0 = x_0/(2v_x)$. This time value, as predicted by the Poiseuille formula, is significantly lower than the experimental values, as evidenced by the results in Fig. 2. Thus, the maximum flow rate of the Poiseuille flow [8] is significantly overestimated for the two systems shown in Fig. 2. For small time values, t_0, Eq. (6) may be used to estimate an approximate overall B value but in the present study individual B values were found by modelling the full trace of the FIA peak, as shown later, which results in a more precise assessment of B.

The velocity of the tail, denoted as v_-, is given by the translatory flow rate (linear flow rate) minus the diffusion velocity, i.e., $v_- = v_x - v_d$. Thus, by the procedure used to estimate the time of onset, the time of segment exit may also be estimated. When the tail distance equals $x_0 + l$ (at positive tail velocity), the time where the tails leave the cell may be approximated by

$$t_- \cong \frac{2}{2v_x + BL_0}x_0 + \frac{2(L_0 + l)}{2v_x + BL_0} \ , \quad 0 < -Bt_- < 1 \ . \quad (7)$$

Thus, the total time where the peak occupies the cell compartment, denoted as the residence time [6], is approximated by subtracting the time of Eq. (6) from the time of Eq. (7)
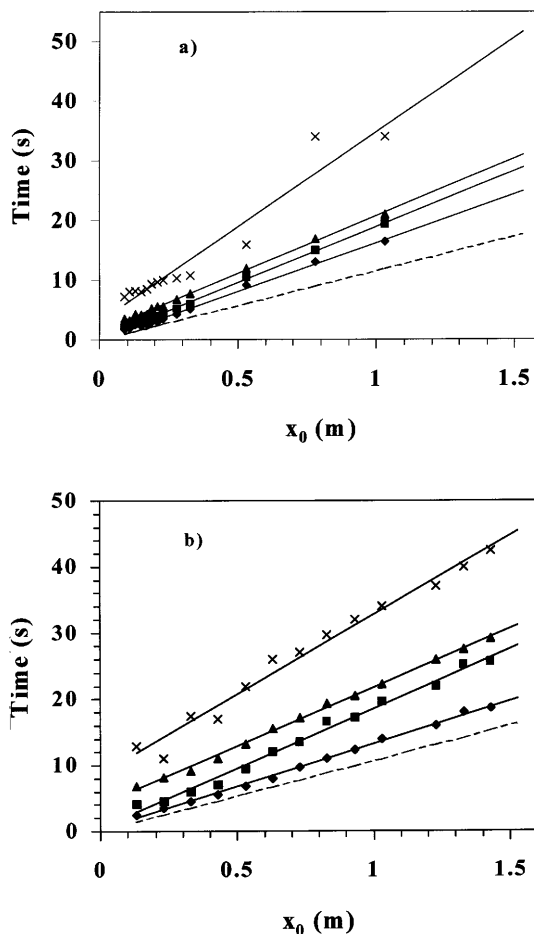
Fig. 2a, b. Time values obtained by fitting the theory (Eqs. 13, 14) to experiment. The *solid lines* indicate a least-squares fit of the data and indicate the almost linear behaviour ($\blacklozenge$)t_0, ($\blacksquare$)t_1, ($\blacktriangle$)t_2, ($\times$)t_3 · **a** Cr^{3+} with $L_0 = 0.058$ m, $v_x = 0.043$ ms^{-1} and $c_0 = 0.002$ M **b** CrO_4^{2-} with $L_0 = 0.168$ m, $v_x = 0.047$ ms^{-1} and $c_0 = 5$ mg/l. The *broken lines* represent the time of onset, as predicted by Poiseuille flow

$$\Delta t \cong \frac{v_x(L_0 + l) - BL_0 x_0}{v_x^2 - \left(\frac{BL_0}{2}\right)^2} \ . \quad (8)$$

An approximate value for the maximum sampling frequency, S_{max}, is therefore obtained by considering the reciprocal value of Eq.(8):

$$S_{max} = \frac{1}{\Delta t} \cong \frac{v_x^2 - \left(\frac{BL_0}{2}\right)^2}{v_x(L_0 + l) - BL_0 x_0} \ , \quad (9)$$

which shows that the maximum sampling frequency is proportional to the flow rate and to the inverse injection-to-cell distance in agreement with earlier results [14]. Note that from Eq. (9), no dependence on concentration is predicted and the maximum sampling time is strongly dependent on the diffusion parameter B. For relatively large values of B, the maximum sampling rate approaches

$$S_{max} \xrightarrow{B \to \infty} - B\frac{L_0}{4x_0} \quad (10)$$

which, of course, is a rough estimate but it shows that in the absence of chemical reactions, the maximum sampling rate is proportional to the diffusion parameter.

3.3 Calculation of The FIA peak

The segment flow, with front and tail velocities, is indicated without diffusion zones in Fig. 1. Because B must be negative, the front velocity approaches infinity when the time approaches infinity. If it is assumed that the mixing zones at the front and at the tail of the flowing segment are equal, the concentration profile within the segment becomes trapezoidal or similar in shape.

From the time of onset and onwards the signal of the peak evolves in a manner defined by the trapezoidal concentration profile convoluted by the exponential function of diffusion (Eq. 1). In terms of time values, the trapezoidal absorbance profile may be described by

$$s(t) = \begin{cases} 0 & 0 \leq t \leq t_0 \\ \frac{1}{(t_1 - t_0)}(t - t_0) & t_0 \leq t \leq t_1 \\ 1 & t_1 \leq t \leq t_2 \\ \frac{1}{(t_2 - t_3)}(t - t_3) & t_2 \leq t \leq t_3 \\ 0 & t_3 \leq t \end{cases} \quad (11)$$

where t_0 is the time of onset and t_1 is the time where the segment reaches maximum absorbance that is maintained until time t_2, where the absorbance starts to decrease until the time of tail exit, t_3. According to Eq. (11), the shape of the absorbance profile is trapezoidal, with slopes at the front and at the back of the segment that are allowed to differ in magnitude. If the detector were monitoring a trapezoidal-shaped segment (absorbance versus time) of a solute with a rapid diffusion rate (compared to the rate of detection), the time derivative of the Beer–Lambert relation (Eq. 1) needs to be considered within the time limits of detection defined by Eq. (11). Accordingly, the shape of the FIA peak may be evaluated by calculating the convoluted signal in each single time interval of Eq. (11), as follows.

$$\tilde{A}(t) = s(t) * \frac{\partial A(t)}{\partial t} = \int_{-\infty}^{\infty} s(\tau) A_0 (-B) \exp[B(t - \tau)] d\tau \ , \quad (12)$$

where $*$ denotes the mathematical procedure of convolution, which yields

$$\tilde{A}(t) = \begin{cases} A_1 \exp(Bt) + A_2 t + A_3 & t_0 < t \leq t_1 \\ A_4 \exp(Bt) + A_5 & t_1 < t \leq t_2 \\ A_6 \exp(Bt) + A_7 t + A_8 & t_2 < t \leq t_3 \\ A_9 \exp(Bt) & t_3 < t \end{cases} \quad (13)$$

where the constants (A_n) are given by

$$A_1 = \frac{A_0}{(t_0 - t_1)B} \exp(-B t_0)$$

$$A_2 = \frac{A_0}{(t_1 - t_0)}$$

$$A_3 = \frac{A_0}{(t_1 - t_0)} \left(\frac{1}{B} - t_0 \right)$$

$$A_4 = \frac{A_0}{(t_1 - t_0)}[\exp(-B t_1) - \exp(-B t_0)]$$

$$A_5 = A_0$$

$$A_6 = -\frac{A_0}{B} \left[\frac{\exp(-B t_0) - \exp(-B t_1)}{t_1 - t_0} + \frac{\exp(-B t_2)}{t_2 - t_3} \right]$$

$$A_7 = \frac{A_0}{(t_2 - t_3)}$$

$$A_8 = \frac{A_0}{(t_2 - t_3)} \left(\frac{1}{B} - t_3 \right)$$

$$A_9 = -\frac{A_0}{B} \left[\frac{\exp(-B t_0) - \exp(-B t_1)}{t_1 - t_0} \right.$$
$$\left. + \frac{\exp(-B t_2) - \exp(-B t_3)}{t_2 - t_3} \right] \ , \quad (14)$$

which, together with Eq. (13), are the fundamental equations of the FIA signal. With A_n, B and t_n applied as fitting parameters Eqs. (13) and (14) may be used to describe the trace of the FIA peak. The time of peak maximum, $t_{\max}$, is found by differentiation of Eq. (13), which yields

$$t_{\max} = \frac{1}{B} \ln \left[-\frac{A_7}{B A_6} \right] \quad (15)$$

and from Eqs. (13)–(15) the absorbance at peak maximum follows:

$$A_{\max} = A_7 \left(t_{\max} - \frac{1}{B} \right) + A_8 \ . \quad (16)$$

Equations (13)–(16) indicate that the calculation of $t_{\max}$ and $A_{\max}$ is cumbersome but reasonable approximations may be introduced by using Eqs. (6) and (7). The time of peak maximum, for the two solutes of the present analysis, was equal to the time t_2 and, in addition, the time of the peak maximum approximately equals the time of the linear flow rate, i.e., $t_{\max} = t_2 \cong x_0/v_x$, which is valid particularly at distances, x_0, longer than 0.2 m.

The important parameter of the present analysis is the B value that accounts for the diffusion process. By varying the flow rates and injection-to-detection distances (x_0) in a large number of experiments and fitting the theory to the data obtained, it was found that the B value depends on flow rate (v_x) but not on distance (x_0). Furthermore, it was found that the B value differed significantly for the two solutes investigated, as portrayed in Fig. 3. The B value was found to depend linearly on the flow rate and the slopes of the lines in Fig. 3 are denoted as α_B, with values given in Table 1:

$$B = \alpha_B v_x \ . \quad (17)$$

Some deviation from straight-line behavior is observed for Cr^{3+} (Fig. 3), which originates from general uncertainties imposed by inevitable oscillations of the peristaltic pump. Also, owing to the level of uncertainty, the intercepts of the lines in Fig. 3 are zero, within experimental error. Since the unit of α_B is m^{-1} it is related to the diffusion coefficient, D, which has the unit $m^2 s^{-1}$ through the relation

$$D = \pi r_0^2 v_x \alpha_B = \partial V / \partial t \ \alpha_B \ . \quad (18)$$
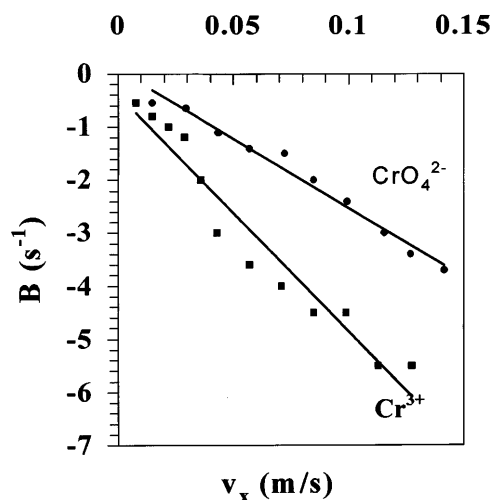
Fig. 3. The B value depicted as a function of linear flow rate. The slope of the lines (α_B) is denoted as the kinematic diffusion coefficient, which was independent of distance (x_0). $x_0(Cr^{3+}) = 0.06$ m and $x_0(CrO_4^{2-}) = 0.4$ m

Table 1. The kinetic diffusion coefficient obtained by fitting Eqs. (13) and (14) to the flow-injection analysis data of Cr^{3+} and of chromate

Species	α_B (m^{-1})
Cr^{3+}	−43(3)
CrO_4^{2-}	−26(1)

Accordingly, in the present description, the diffusion coefficient becomes proportional to the flow rate, which indicates that it is not a universal constant. It should be noted that it is not possible to determine the diffusion coefficient at zero flow rate in the present work, since this would require that the intercepts of the lines in Fig. 3 were determined with good precision. Such work is in progress using piston pumps that exhibit much smaller variations and oscillations in flow rate and it is expected that the magnitude of the intercept should be found in the range between 0.01–0.1 s^{-1}, if it were to be comparable with literature values. The result of Eq. (17) may be introduced into all the previous equations, which, for example, confirms that S_{max} (Eq. 9) becomes proportional to the flow rate.

Some of the results of the analysis are depicted in Fig. 4, where good correspondence between theory and experiment is observed for three distances (x_0). All the features of the FIA trace are reproduced by theory but with smaller deviations between theory and data observed only at the outermost section of the tail (right-hand side of the peaks).

The t_n values also emerge from the procedure of fitting theory to experiment, as shown in Fig. 2, where they are depicted as a function of distance, x_0. Apparently, all the t_n values depend linearly on x_0 and, although a slight curvature may be identified, the intercepts of the t_0 lines are zero, within experimental error. Thus, the linear dependence prevails, as predicted by Eqs. (6) and (7). In Fig. 2, it should be noted that the lines of t_1 and t_2 are
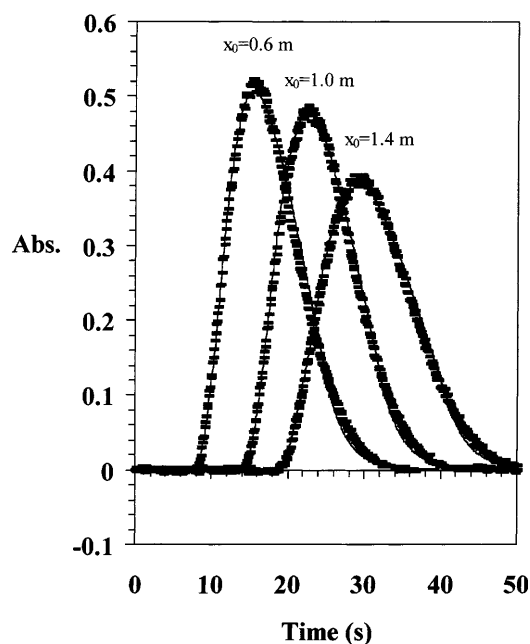
Fig. 4. Results of fitting the theory (*solid line*) to experiments with chromate (*horizontal bars*) at three different distances (x_0). Conditions given in Fig. 2

parallel, which shows that the central core of the segment neither expands nor contracts during the flow. The time separation between the lines corresponds well to the time required for the initial length of the segment, L_0, to pass the detector at the velocity of the linear flow rate. The time separation of Cr^{3+} was 1.2(3) s while that of chromate was 3.6(3) s. This result shows that there is always an inner core of the segment which remains unaltered in length during the flow. The extension of the segment may then be visualised as an initial length of the segment that expands both in the forward and in the backward direction during flow, as a result of simple diffusion (Eq. 2). Within the core of the segment, and at a given time, there was no concentration gradient, i.e., the absorbance was constant within the inner core. By using the approximate value of t_2 and the fact that the length of the central core of the segment equals L_0, the estimated value of t_1 becomes $(x_0 - L_0)/v_x$. The results of t_3 for Cr^{3+} (Fig. 2a) show some deviation from a straight line, particularly at large distances. This deviation is a result of the relatively small peak heights at large distances (x_0), which make the determination of t_3 slightly uncertain. However, the slopes of the lines in Fig. 2 show that the shape of the absorbance profile is asymmetric and trapezoidal.

Figure 5 illustrates schematically how the concentration and the extension of the segment develops while it flows. It shows that the segment is diluted while it expands and that mixing zones develop with a large linear concentration gradient at the front and a numerically smaller linear concentration gradient at the tail. The midsection of the segment travels at the speed of the linear flow rate, as determined by the volumetric flow rate. The reason that the leading edge reaches the detector much earlier than given by the time of the linear

Direction of flow
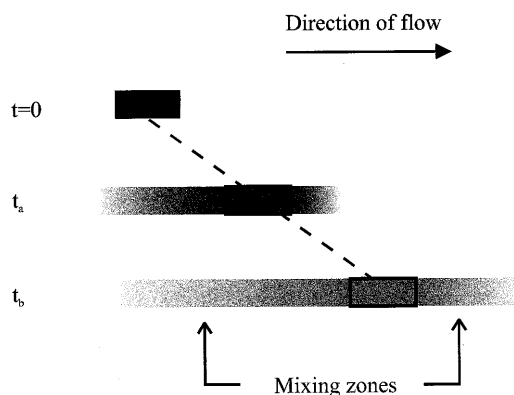
Fig. 5. Schematic illustration of the segment length and concentration (*shades*) development as a function of time. The size of the inner core remains unaltered in length (indicated by *solid area*) while mixing zones develop during flow at the front and at the tail $0 < t_a < t_b$

flow rate is suggested to be related to simple diffusion and not as a result of Poseuille flow [8]. In a system with modified Poiseuille flow, Narusawa [9] also introduced concentration gradients at the front and at the tail of the segment which account for the curve of zone-circulating FIA (ZCFIA); however, the time of arrival of the leading edge in ZCFIA does not fit the results of the present experiments (Fig. 2). Furthermore, with Poiseuille flow, Korenaga et al. [8] showed that the absorbance of the tail section of the FIA response becomes proportional to the inverse time, which is different from the present results, where the tail absorbance falls off exponentially (Eqs. 15, 16), in accord with earlier results [1, 7]. In the original FIA publication by Ryzicka and Hansen [1], the tail section of the FIA decays exponentially, following the function $A = E \exp\left(-\frac{t}{b}\right)$, $t > t_3$, where E and b are constants. In the present context (Eqs. 13, 14), the constants take the values $E = A_9$ and $b = -\frac{1}{B}$ but apart from this correspondence the similarities among the two models are weak. Vanderslice et al. [10] provided formulae that account for the time of initial appearance and a baseline-to-baseline time, which, in the present description, correspond to t_0 (Eqs. 5, 6) and to Δt (Eq. 8), respectively. It was found that

$$t_0 = 109 r_0^2 D^{0.025} \left(\frac{x_0}{v_x}\right)^{1.025}$$

and that

$$\Delta t = \frac{35.4 r_0^2}{D^{0.36}} \left(\frac{x_0}{v_x}\right)^{0.64},$$

[10], where the denotations of the present analysis are used. When $B = \alpha_B v_x$ is introduced into Eq. (6), the time of arrival of the leading edge becomes proportional to the inverse flow rate and to the distance travelled, but is independent of the tube radius. Similar observations apply to the residence time (Eq. 8) and the major discrepancies between the two models are associated with the substitution of the static diffusion coefficient (D) for the dynamic diffusion coefficient (α_B) as well as the dependence, or lack of dependence, on tube radius. Especially, the dependence on tube radius, which is tube

radius squared, is very strong and ought to be easily verified experimentally, but the dependence seems not to be fully justified [10]. Attempts to switch between two tube radii, $r_0 = 2.5 \times 10^{-4}$ and 5.0×10^{-4} m (in the present analysis) did not confirm the proportionality to the radius squared but, on the other hand, yielded equal time values. Whether or not this result is linked to differences in tube roughness, for example, remains to be clarified.

The present model shows that the concept of streamlines is inconvenient and that the flow should be understood as segment flow, where the mixing of solute with solvent originates solely from simple diffusion. A FIA peak may then be described without including the concepts of microturbulence and radial diffusion [9]. The asymmetry of the peak is ascribed to friction between the solute and the walls, which effectively delays some of the solute molecules with respect to the bulk of the segment.

One of the implications of the model is that to a large extent the peak shape is defined by the diffusion process together with the actual method of measurement. No concentration gradients within the segment were predicted, apart from the front section and the tail section of the travelling segment. Therefore, for a segment of a given concentration, the peak may attain several shapes dependent on the physical configuration of the system. The equations above predict that the FIA peak does not change shape upon injection of segments of different concentrations for given pump rates, tube lengths, etc. Furthermore, the equations show that it becomes possible to establish absolute amounts of solute in the detection cell at a given time. Tentatively, experiments that monitor the number of absorbing species may be performed. Thus, in principle, the method may also be applied to establish the amount of interference present.

The theory implies that it is advantageous to use short distances (x_0) to increase the sampling rate (Eq. 9). Of course, this is true only for systems without chemical reactions, where the absorbance decreases exponentially right from the point of injection. If chemical reactions were proceeding, several additional effects, such as an initial time of mixing of chemicals, time of reaction, change of temperature, etc., must be included in order to estimate the maximum sample frequency.

3.4 The chemical reaction

In the previous sections systems with simple diffusion were treated and the theory describes satisfactorily the shape of FIA peaks where no chemical reactions are involved. Therefore, it is also feasible to investigate a system where a sample is injected into a stream of chemicals and, subsequently, to monitor the response of the product formed by the reaction. The reaction of chromate with DPC [12, 13] was chosen as an example of such a system. This reaction forms a pink product which was detected at 548 nm. The reaction imposed a higher background level with greater variations compared to measurements performed with pure solutes (above). As opposed to the study of pure solutes (Fig. 4), the FIA peak height did not decrease exponentially with distance.

Dependent on the reaction kinetics, the peak height increased from the point of injection where the reaction commenced and the product was formed. When the chemical reaction finished the FIA peak height reached a maximum and from this point onwards the peak height of the product fell off according to simple diffusion (Eq. 1). In the case of a chemical reaction, the theory also describes satisfactorily the trace of the FIA peak (Fig. 6). It was found that a maximum amount of product was formed after the sample had travelled a distance of approximately 2 m and that after this point the peak height decreased as shown for the peak height at $x_0 = 3.5$ m (Fig. 6). The parameters obtained by the adaptation of theory to experiment (Fig. 6) are given in Table 2 and they show that the segment profile of the absorbance was almost triangular, as evidenced by the similarity of t_1 and t_2 (Table 2). The areas under the curves in Fig. 6 are equal with the value 3.3(1) A s, which supports the notion that the total amount of product monitored remained constant after completion of the reaction. The reaction kinetics of the system is currently under investigation but the understanding of the system is complicated by the instability of the chromium-DPC chelate formed [13]: once formed, it deteriorates, thus producing smaller peak heights than expected from simple diffusion. Furthermore, large differences were observed between straight reaction tubes and coiled reaction tubes (not shown); however, the theory shows that the individual FIA peaks are well understood, which allows detailed studies of chemical reactions as they proceed within the tubes. The FIA peaks were described earlier [15, 16] by a Gaussian–Lorentzian model, which is fundamentally different from the results of the present analysis, but at large distances and relatively low flow rates the FIA peak may be approximated by, for example, a Gaussian distribution (Table 2). The absorbances (A_0) in Table 2, as fitted to
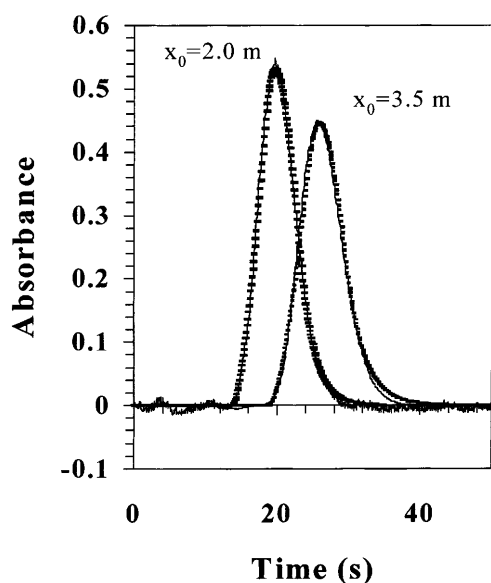
Table 2. Parameters of Eqs. (13) and (14) obtained by fitting theory to experiment, as shown in Fig. 6. Also shown are the parameters (N, μ, σ) of an adaptation to the results of the Gaussian distribution $G(x) = N/\sqrt{2\pi}\sigma \, \exp(-(x - \mu)^2/2\sigma^2)$

Parameter	$x_0 = 2.0$ m	$x_0 = 3.5$ m
A_0 (A)	0.32	0.24
B (s^{-1})	−0.46	−0.40
t_0 (s)	13.5	18.6
t_1 (s)	18.0	24.0
t_2 (s)	19.1	24.4
t_3 (s)	22.3	29.3
N (A)	3.7	3.0
μ (s)	18.4	25.8
σ (s)	22.3	29.3
Area	3.3(1)	3.2(1)

experimental results, exhibit lower values compared to the values seen in Fig. 6. This is a characteristic feature of the FIA peaks of the chemical reaction and is, as of yet, not fully investigated.

4 Conclusion

A description of the flow in a FIA system was developed and the model supplies parameters relating to simple diffusion. It was shown that diffusion within the FIA manifold may be characterised by a diffusion coefficient (Eq. 17), denoted as the kinematic diffusion coefficient (α_B), that is related to the common "stationary diffusion coefficient" (D) through Eq. (18). For the two systems investigated, the values of α_B differed by a factor of 2. The flow type is suggested to be "pluglike" or segmental in the FIA manifold where solvent molecules diffuse into both the front and tail during the flow and the solute molecules diffuse away from the centre of gravity of the segment. The concentration profile of the segment during flow was trapezoidal where the gradient at the front is higher than the gradient at the tail. The approximate time values that characterise the concentration profile were t_0 (Eq. 6), $t_1 \cong (x_0 - L_0)/v_x$, $t_2 \cong x_0/v_x$ and t_3 (Eq. 7). It was shown that the description (Eqs. 13, 14) reproduces well the traces of FIA profiles both for systems of simple diffusion and for systems of chemical reactions. Formulae for the time of onset, residence time, maximum sampling frequency and FIA peak shape followed from the theory. It is suggested that the theory may be used in favour of, for example, Gaussian profiles to resolve the contribution of interference to the analyte signal. In addition, it may be used as a tool in the investigation of molecular dynamics such as the kinetics of chemical reactions.

Fig. 6. FIA peaks of the chromate-diphenylcarbazide reaction (see text) for two distances (x_0) at which the chemical reaction was completed. $L_0 = 0.15$ m, $r_0 = 2.5 \cdot 10^{-4}$ m, $v_x = 0.1$ ms^{-1}

References

1. Ruzicka J, Hansen EH (1975) Anal Chim Acta 78: 145
2. Ruzicka J, Stewart JWB (1975) Anal Chim Acta 79: 79

416

3. Ruzicka J (1994) Analyst (Cambridge) 119: 1925
4. Scampavia LD, Blankenstein G, Ruzicka J, Christian GD (1995) Anal Chem 67: 2743
5. Hodder PS, Blankenstein G, Ruzicka J (1997) Analyst (Cambridge) 122: 883
6. Ruzicka J, Hansen EH (1988) Flow injection analysis, 2nd edn. Wiley, New York
7. Nagy F, Fehér ZS, Pungor E (1970) Anal Chim Acta 52: 47
8. Korenaga T, Yoshida H, Yokota Y, Kaseno S, Takahashi T (1986) J Flow Injection Anal 3: 91
9. Narusawa Y (1998) J Flow Injection Anal 15: 9
10. Vanderslice JT, Rosenfeld AG, Beecher GA (1986) Anal Chim Acta 179: 119
11. Hulsman M, Bos M, van der Linden W (1997) Anal Chim Acta 346: 351
12. Andersen JET (1998) Anal Chim Acta 361: 125
13. de Andrade JC, Rocha JC, Baccan N (1985) Analyst (Cambridge) 110: 197
14. Ruzicka J, Hansen EH (1983) Anal Chim Acta 145: 1
15. Wu X, Bellgardt K-H (1995) Anal Chim Acta 313: 161
16. Novic M, Novic M, Zupan J, Zafran N, Pihlar B (1997) Anal Chim Acta 348: 101